International Journal of Biological Macromolecules 269 (2024) 131951

Contents lists available at ScienceDirect

International Journal of Biological Macromolecules

journal homepage: www.elsevier.com/locate/ijbiomac

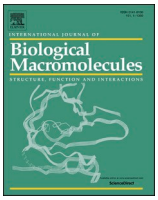

Effect of the *ex situ* physical and *in situ* chemical modification of bacterial nanocellulose on mechanical properties in the context of its potential applications in heart valve design

Alicja Stanisławska [a,*], Marek Szkodo [a], Hanna Staroszczyk [b], Kinga Dawidowska [d], Magdalena Kołaczkowska [c], Piotr Siondalski [c]

[a] Department of Mechanical Engineering and Ship Technology, Gdańsk University of Technology, Narutowicza 11/12 St., 80-233 Gdańsk, Poland
[b] Department of Chemistry, Technology and Biotechnology of Food, Chemical Faculty, Gdańsk University of Technology, Narutowicza 11/12 St., 80-233 Gdańsk, Poland
[c] Department of Cardiac and Vascular Surgery, Medical University of Gdańsk, Dębinki 7 St., 80-211 Gdańsk, Poland
[d] Medical Engineering Division, Maritime Advanced Research Centre, Szczecińska 65 St., 80-392 Gdańsk, Poland

ARTICLE INFO

Keywords:
Bacterial cellulose
In situ and *ex situ* modification
Mechanical properties

ABSTRACT

Bacterial nanocellulose (BNC) is a promising material for heart valve prostheses. However, its low strength properties limit its applicability in cardiovascular surgery. To overcome these limitations, the mechanical properties of BNC can be improved through modifications. The aim of the research was to investigate the extent to which the mechanical properties of BNC can be altered by modifying its structure during its production and after synthesis. The study presents the results of various analyses, including tensile tests, nanoindentation tests, X-ray diffraction (XRD) tests, scanning electron microscopy (SEM), Fourier-transform infrared spectroscopy (FTIR) and Raman spectroscopy, conducted on BNC chemically modified *in situ* with hyaluronic acid (BNC/HA) and physically modified *ex situ* through a dehydration/rehydration process (BNC 25DR, BNC105DR, BNC FDR and BNC/HA 25DR, BNC/HA 105DR, BNC/HA FDR). The results demonstrate that both chemical and physical modifications can effectively shape the mechanical properties of BNC. These modifications induce changes in the crystalline structure, pore size and distribution, and residual stresses of BNC. Results show the effect of the crystalline structure of BNC on its mechanical properties. There is correlation between hardness and Young's modulus and $I\alpha/I\beta$ index for BNC/HA and between creep rate of BNC/HA, and Young's modulus for BNC *vs* $I\alpha/I\beta$ index.

1. Introduction

According to estimates from the American Heart Association (AHA), approximately 5 million individuals in the United States are diagnosed with heart valve disease, and this condition is responsible for tens of thousands of deaths annually. However, these figures may not reflect the global burden of the disease. The World Health Organization (WHO) identifies rheumatic heart disease as a leading cause of heart valve problems, particularly in low-income and middle-income countries. Additionally, degenerative valve diseases, such as calcific aortic valve stenosis, are becoming increasingly prevalent, particularly in aging populations. Therefore, efforts are constantly being made to find solutions for the development of new alternative materials and constructions that would allow for the design of a new innovative heart valve, free from the shortcomings of mechanical and biological valves currently used by the healthcare service. One of these materials could be bacterial nanocellulose (BNC).

Cellulose, a polysaccharide derived from D-glucose units, exists naturally and can be produced by bacteria, notably *Komagataeibacter xylinus* [1,2]. BNC offers unique properties making it valuable for various applications in medicine and technology, such as dressing materials, blood vessel implants, and artificial skin [3–6]. However, BNC's mechanical strength is relatively low, due to its high water content [7,8]. To address this limitation, physical or chemical modification techniques can be employed [9]. Physical modification through drying methods [10–12], including *ex situ* dehydration and rehydration, enhances BNC's tensile strength without compromising its elasticity [13]. These modifications are crucial, especially in the development of

* Corresponding author.
E-mail address: alicja.stanislawska@pg.edu.pl (A. Stanisławska).

https://doi.org/10.1016/j.ijbiomac.2024.131951
Received 8 January 2024; Received in revised form 24 April 2024; Accepted 26 April 2024
Available online 6 May 2024

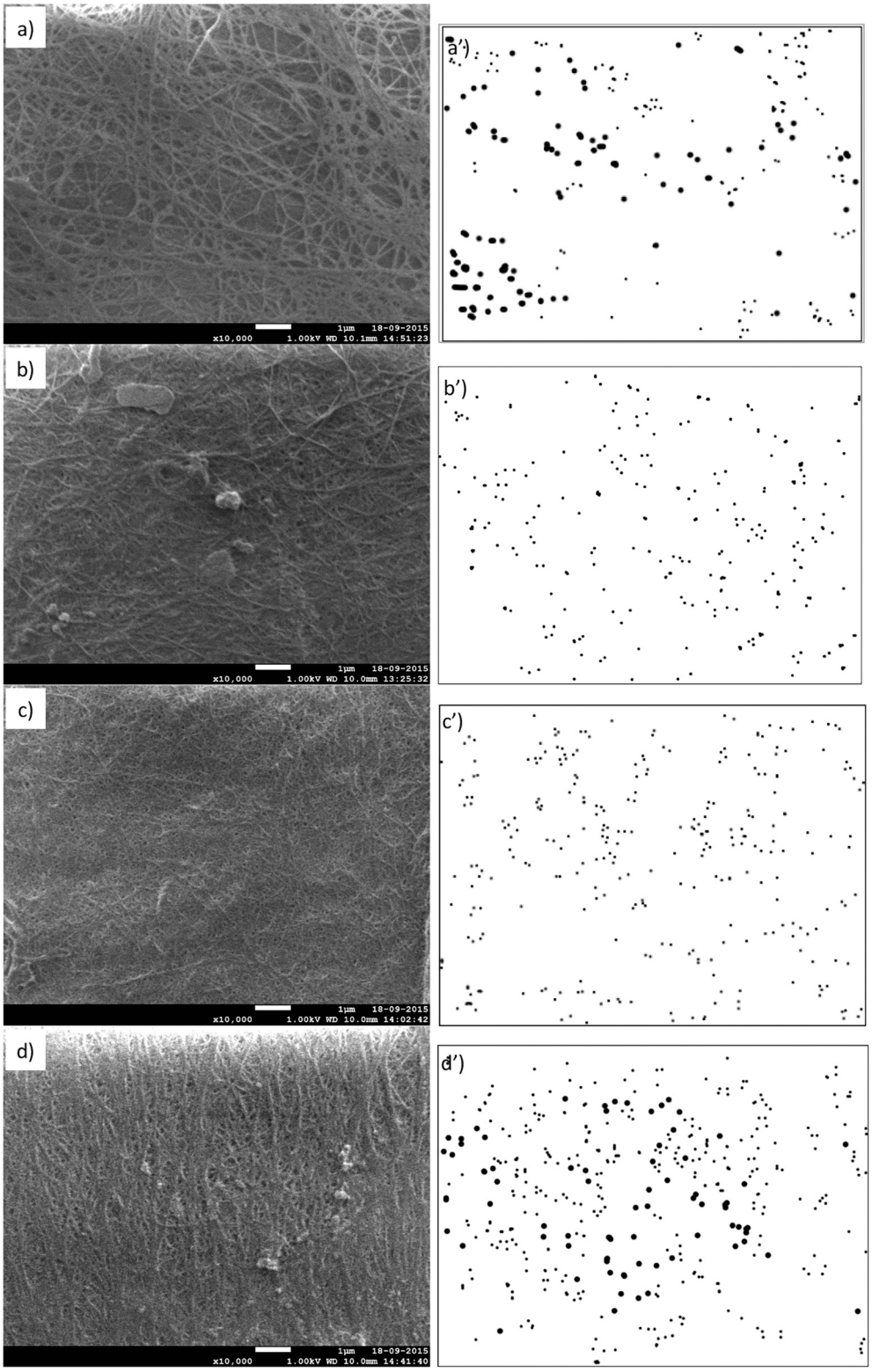

Fig. 1. The SEM images of: a) BNC b) BNC 25DR, c) BNC 105DR d) BNC FDR. a′), b′), c′), d′) binary images of pores in structures.

personalized artificial heart valves [12,14].

Chemical modification methods offer possibilities to enhance the structure and properties of bacterial nanocellulose (BNC). *In situ* synthesis enables the integration of various compounds like chitosan, sodium alginate, or potato starch during BNC production, improving its characteristics [15–17]. Surface modification techniques, such as cross-linking reactions or treatments like acetylation, phosphorylation, or boiling in sodium hydroxide solution, can enhance specific properties of BNC [18–21]. Incorporating hyaluronic acid (HA) into the cellulose matrix can also improve BNC's mechanical and functional properties, potentially enhancing its biocompatibility [22]. *In situ* modification with HA during BNC synthesis can lead to copolymerization, potentially improving its strength properties. While studies have focused on the physicochemical and structural properties of HA-modified BNC, it is

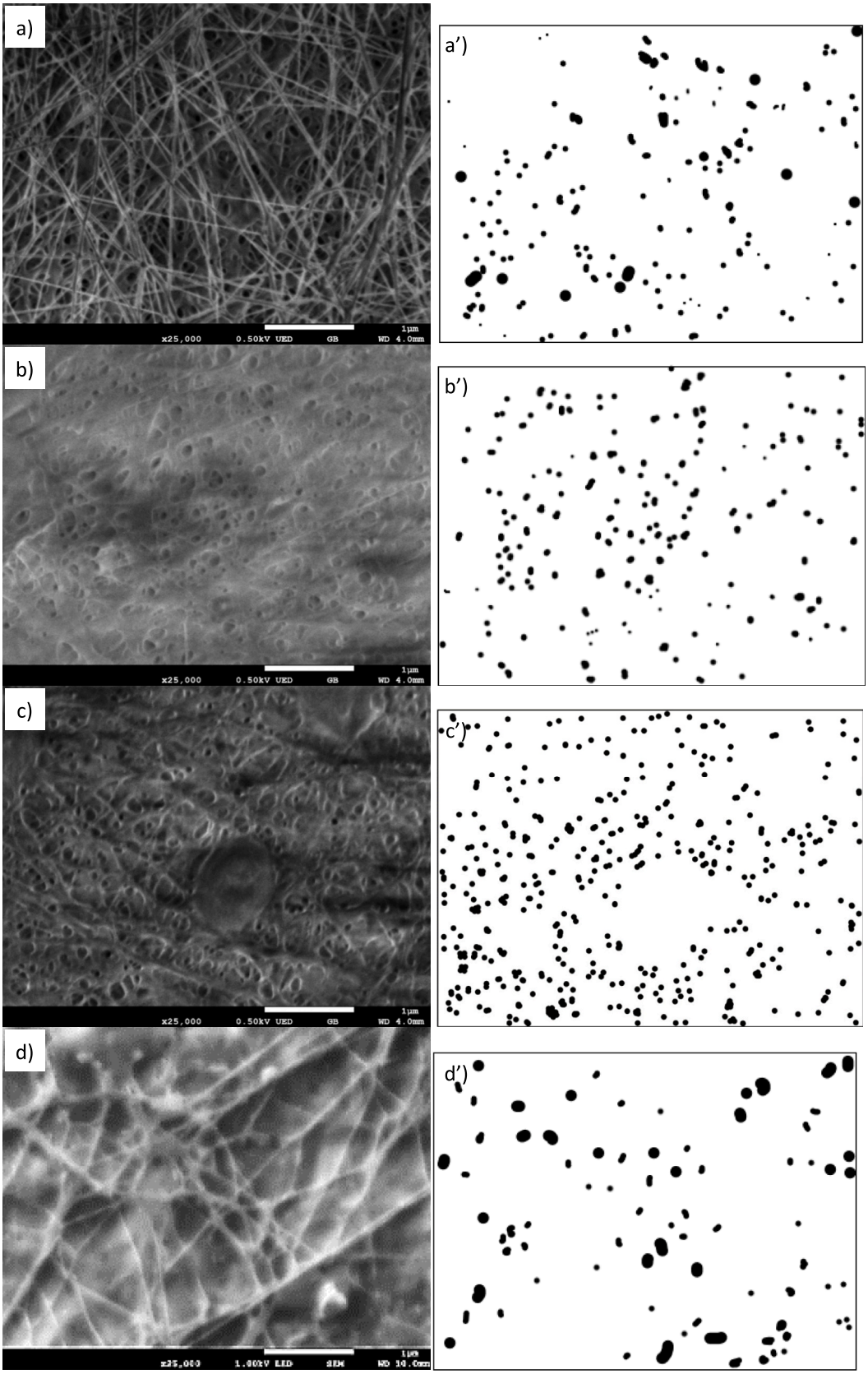

Fig. 2. The SEM images of: a) BNC/HA; b) BNC/HA 25DR, c) BNC/HA 105DR d) BNC/HA FDR. a′), b′), c′), d′) binary images of pores in structures.

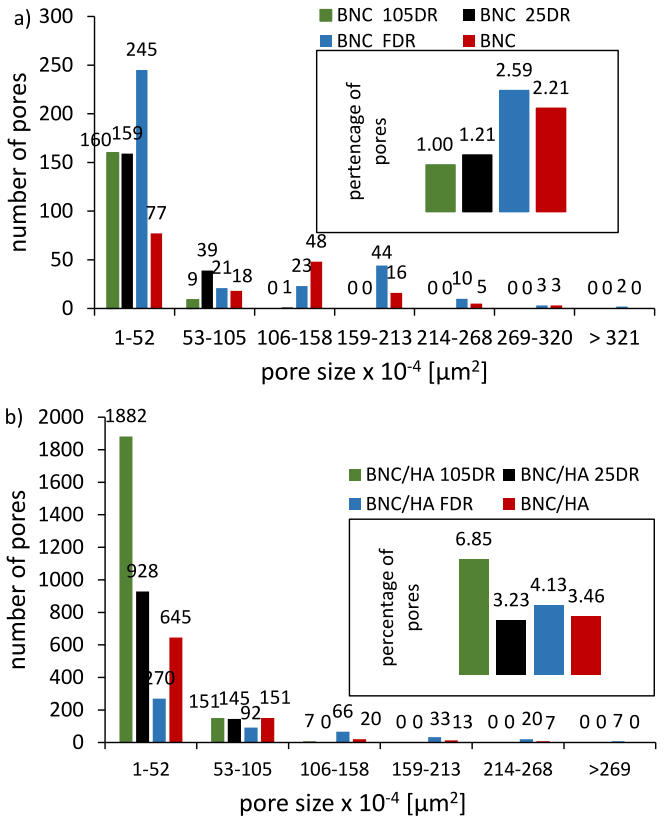

Fig. 3. Percentage of pores and their distribution for BNC - a) and BNC/HA - b). Pores were counted from an area of 114.8 µm^2.

believed that HA presence can positively influence the mechanical performance of the composite [23–25]. Hyaluronic acid also accelerates the healing process of chronic wounds and acts as an anti-inflammatory agent [26]. *Ex situ* modification involves blending bacterial nanocellulose (BNC) and hyaluronic acid (HA) to create composite materials, known to exhibit higher tensile strength compared to BNC alone due to strong hydrogen bond formation [24,27]. However, this method is costly and labor-intensive. Alternatively, *in situ* modification of BNC/HA can be achieved by adding HA to the bacterial medium during synthesis, followed by drying and rehydration [22].

The proper selection of appropriate chemical and physical modifications for bacterial nanocellulose (BNC) can greatly improve its mechanical properties, such as tensile strength and creep resistance. These properties are crucial for cardiovascular implants, including aortic heart valves, which are subjected to varying stress conditions [28]. In addition to enhancing mechanical performance, the chosen modifications can also increase the biocompatibility of BNC [29]. This is important for ensuring the safety and longevity of valve prostheses made from BNC. By improving the material's biocompatibility, the risk of adverse reactions or complications can be minimized.

This article presents a study on the mechanical properties of bacterial cellulose (BNC) and its *in situ* modification by adding hyaluronic acid (HA) to the bacterial medium. Additionally, both forms of BNC were further modified *ex situ* through different drying methods: water soaking with convection drying at 25 °C and 105 °C, as well as freeze-drying.

The aim of the study was to investigate whether chemically modified bacterial nanocellulose, modified *in situ* using HA and then subjected to dehydration and rehydration processes, meets the requirements for mechanical properties for use in artificial heart valves. In order to achieve this goal, a tensile test was conducted (to determine tensile strength and elongation at break), as well as instrumental indentation technique (to determine hardness, longitudinal modulus of elasticity, and creep velocity), and X-ray diffraction analysis, which allowed for the application of the Williamson-Hall method to determine the intrinsic stresses present in each modification applied. The findings of the study contribute to a better understanding of the factors influencing changes in the mechanical properties of BNC when modifications are applied. By elucidating the relationship between modifications, structural alterations, and mechanical performance, the study highlights the potential of BNC as a biomaterial for aortic artificial heart valves.

2. Materials and methods

2.1. Materials

Samples for testing the mechanical properties of BNC were produced by the biotechnology company BOWIL Biotech Ltd. The process of cellulose production is extensively described in the patents PL 171952B1 (1993) and PL 212003B1 (2003). The complete details of producing native BNC are presented in the research conducted by [12].

The production of BNC involved using a strain of *Komagataeibacter xylinus* E25 and a standard Schramma and Hestrina (SH) solution, which consisted of 20 g/L glucose, 5 g/L yeast extract, 5 g/L peptone, 2.7 g/L disodium phosphate, 1.15 g/L citric acid monohydrate, 0.5 g/L magnesium sulfate, as well as 5 g/L aminobak. The solution consisted of 5–10 % inoculum, which constituted 1/3 of the total volume. The synthesis temperature ranged from 30 ± 2 °C, and the pH of the medium was maintained at 5.75 ± 0.03. The standard culture lasted for 3 days and was conducted in a horizontal reactor with an area of 0.05 m2

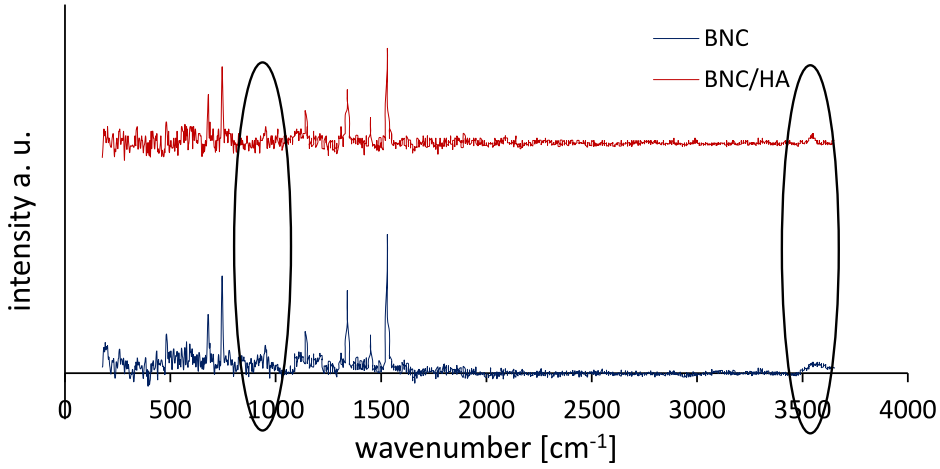

Fig. 4. Raman spectrum for BNC and BNC/HA.

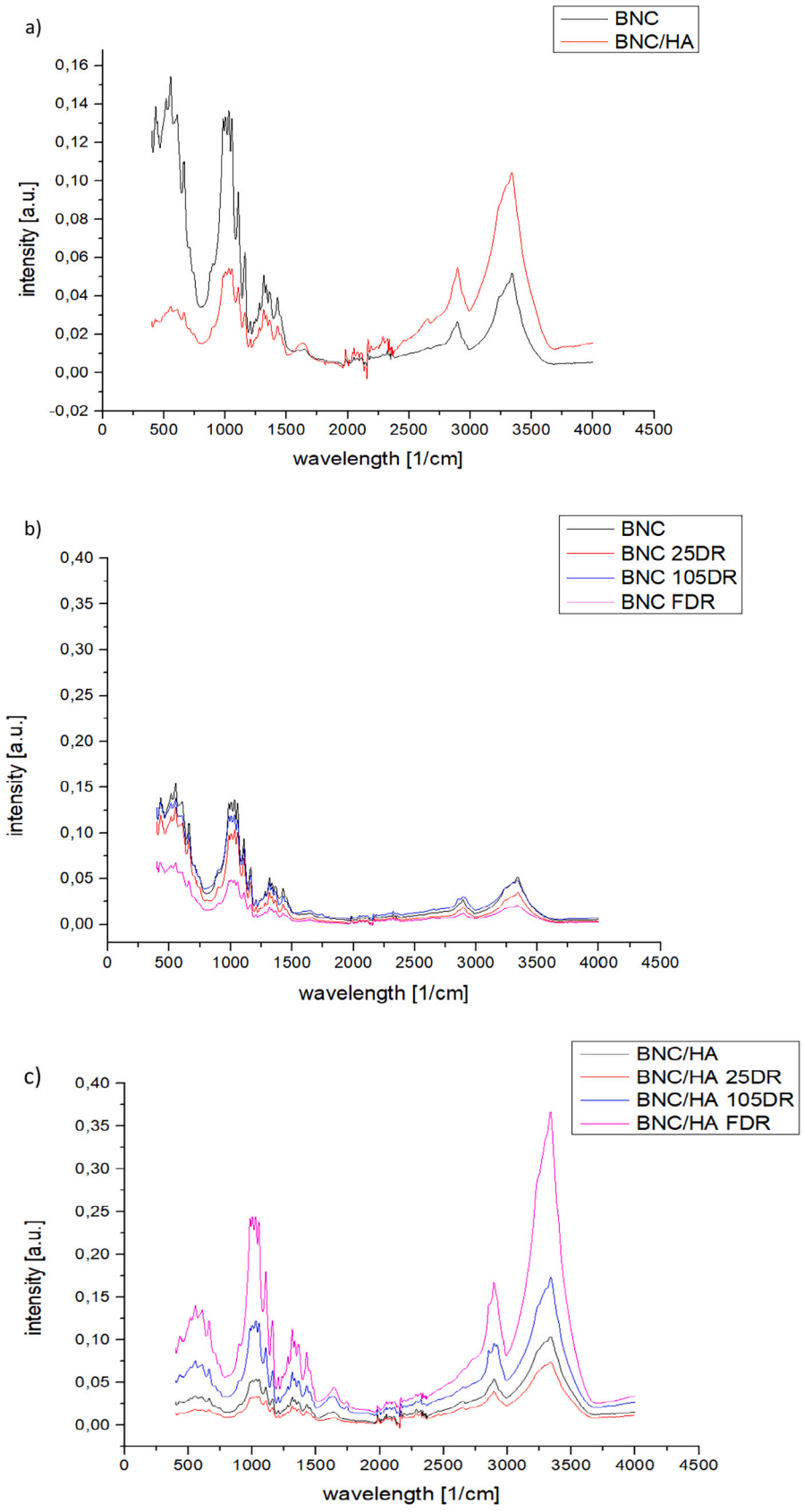

Fig. 5. FTIR spectrum for native BNC and BNC/HA – a), *ex situ* modified BNC – b), *ex situ* modified BNC/HA – c).

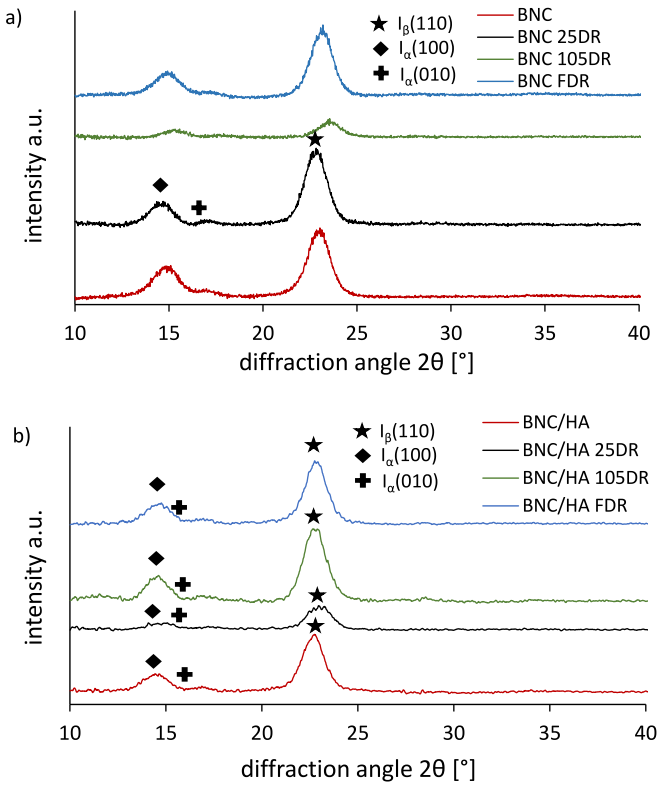

Fig. 6. X-ray diffraction images for native *ex situ* and physically modified BNC for native - a), and *ex situ* physically modified BNC/HA - b).

placed in a tray with openings to facilitate oxygen flow. The tray contained the HS solution with the addition of aminobak and was incubated with a 5–10 % (*v*/v) suspension of the bacterium *G. xylinus* E25. After 7 days of surface culturing, a highly hydrated BNC membrane was formed. After the synthesis process, the membranes were purified, compressed, rinsed with water, and boiled four times for 1 h at 80 °C. The first boiling was performed in 1 % sodium hydroxide (NaOH), followed by subsequent boiling in acetic acid, tap water, and deionized water, respectively. After each cellulose boiling process, excess water was removed by applying a pressure of 345 kPa. In the subsequent step of the synthesis, the cellulose was sterilized in an autoclave at a temperature of 120 °C for 20 min. The resulting cellulose had a thickness of 2 mm, was wet, and could not be used for XRD tests, Raman spectroscopy, SEM, and nanoindentation. To enable these tests, the cellulose was dried at 20 °C for 48 h. However, wet cellulose was utilized for tensile testing.

To produce chemically modified BNC, the production process was carried out in SH medium containing 2 % glucose and 1 % HA (Hyaluronic Acid) added during the tray casting stage, which allowed for *in situ* modification.

Following the modification stage, the same steps as those used for native BNC synthesis were followed. The resulting material was then cut into smaller pieces and sterilized in an autoclave at 120 °C for 20 min. This material was intended for testing in a tensile test. For XRD, Raman spectroscopy, SEM, and nanoindentation tests, separate samples were dried at 20 °C for 48 h. These samples represented the modified material, specifically native BNC/HA, and had a thickness of 2 mm.

To create physical modifications, both the native BNC and BNC/HA materials were subjected to dehydration and subsequent rehydration processes. For dehydration, convection drying was performed at different temperatures: 25 °C (25DR), 105 °C (105DR), and freeze-drying (FDR). After the dehydration process, the materials were rehydrated by soaking them in demineralized water at 25 °C for 2 h. This rehydration step is known as *ex situ* modification. The resulting samples had different thicknesses depending on the dehydration method used. For 25DR and 105DR, the samples had a thickness of 0.5 mm. For FDR, both BNC and BNC/HA samples had a thickness of 2 mm.

2.2. Methods

2.2.1. Scanning electron microscopy analysis (SEM)

The morphology of the modified BNC samples was examined using a scanning electron microscope (SEM) model JSM 7800-F, manufactured in Tokyo, Japan. To observe the non-conducting cellulose effectively, the microscope operated at a low electron beam accelerating voltage of 0.5 and 1 kV. The electron gun current used during the study was set at 65 pA.

The examination of BNC morphology was conducted at magnifications of 10,000× and 25,000×, respectively. By capturing images of the BNC microstructure after various modification methods, the porosity of the material was calculated. This involved binarizing the monochromatic images and analyzing the quantity and distribution of pores using the MultiScan software, which is an Advanced Image Input and Analysis System developed by CSS-Ltd. in Warsaw, Poland.

2.2.2. Raman spectroscopy analysis

The Raman system employed in the study was equipped with a continuous-mode laser with a wavelength of 360 nm and a power output of 1000 mW. To excite the sample, a laser beam with a power of 500 mW

Table 1
Results of XRD diffraction pattern analysis for BNC and BNC/HA after various modification processes. B - half peak broadening, A - area under the peak, ± standard error.

	(100)			(010)			(110) or (200)			*Iα/Iβ*	Cr.I.	Z
	2θ	B	A	2θ	B	A	2θ	B	A			
BNC	14.85 ±0.01	1.39 ±0.02	793.01 ±8.91	16.75 ±0.04	2.21 ±0.11	317.54 ±4.55	22.96 ±0.00	1.19 ±0.01	1553.00 ±7.71	0.51 ±0.0063	91.00 ±0.42	−16.64
BNC 25DR	14.60 ±0.01	1.43 ±0.03	683.58 ±9.40	16.90 ±0.03	2.00 ±0.09	277.99 ±6.18	22.81 ±0.00	1.20 ±0.01	1752.00 ±7.84	0.39 ±0.0056	90.30 ±0.38	4.75
BNC 105DR	15.32 ±0.01	1.04 ±0.04	130.51 ± 3.34	17.74 ±0.04	1.08 ±0.10	28.07 ±1.79	23.56 ±0.01	1.12 ±0.02	323.00 ±3.44	0.40 ±0.0112	51.13 ±0.51	−21.00
BNC FDR	14.90 ±0.01	1.28 ±0.03	547.97 ± 9.37	17.12 ±0.03	1.40 ±0.10	96.93 ±3.15	23.13 ±0.00	1.10 ±0.01	1414.00 ±8.66	0.39 ±0.0070	89.00 ±0.51	−9.77
BNC/HA	14.47 ±0.01	1.45 ±0.03	294.70 ±5.09	16.80 ±0.03	1.45 ±0.10	70.63 ±2.72	22.68 ±0.00	1.20 ±0.01	800.00 ±4.37	0.37 ±0.0067	78.86 ±0.40	11.13
BNC/HA 25DR	14.77 ±0.02	1.50 ±0.09	107.30 ±4.80	17.28 ±0.07	1.49 ±0.21	37.55 ±3.53	22.99 ±0.01	1.27 ±0.02	347.00 ±3.93	0.31 ±0.0143	48.38 ±0.51	3.33
BNC/HA 105DR	14.53 ±0.01	1.16 ±0.03	324.84 ±6.89	16.96 ±0.05	1.17 ±0.14	51.24 ±3.51	22.76 ±0.00	1.13 ±0.01	993.00 ±6.68	0.33 ±0.0073	83.90 ±0.53	11.33
BNC/HA FDR	14.61 ±0.01	±1.34 ±0.03	312.55 ±4.94	17.00 ±0.04	1.25 ±0.12	75.60 ±2.85	22.81 ±0.00	1.15 ±0.01	855.00 ±4.33	0.37 ±0.0061	80.93 ±0.38	6.81

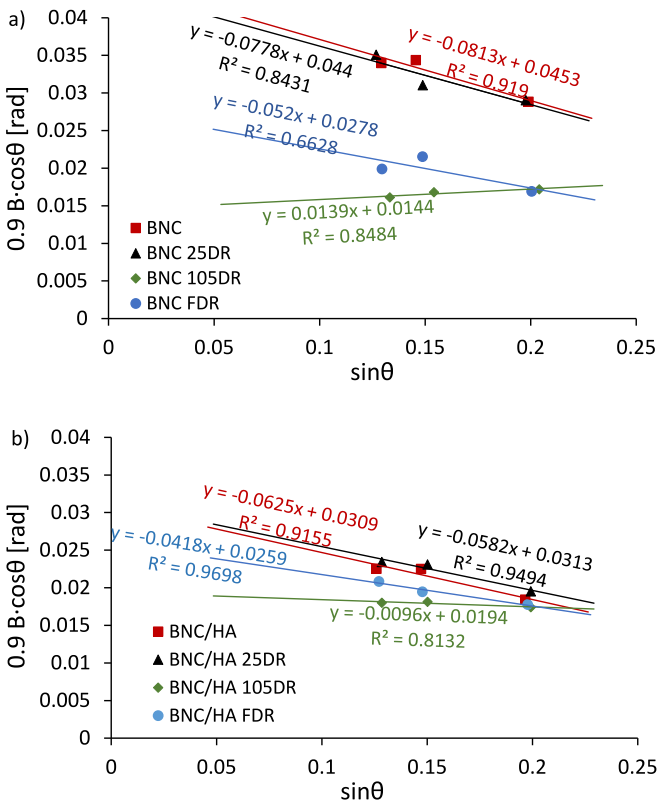

Fig. 7. Williamson-Hall analysis for native BNC and its modifications - a), and for BNC/HA and its modifications - b).

was utilized. The laser beam fell on the sample at a 90-degree angle. The Raman scattering collection time for each measurement was set at 30 s. Raman spectra were collected for both the BNC and BNC/HA samples under identical experimental conditions. This ensures consistency in the measurements and allows for direct comparison of the Raman spectra obtained from the two investigated samples.

2.2.3. Fourier-transform infrared spectroscopy analysis (FTIR)

The spectra were recorded on a Nicolet 8700 spectrometer in the range of 400 to 4000 cm^{-1}. Measurements were conducted using a Golden Gate ATR accessory with a single reflection on a diamond crystal. The temperature during measurements was maintained at 25 ± 0.1 °C. Each spectrum consisted of 128 scans at a resolution of 4 cm^{-1}. Turbo mode lighting was used during measurements. Prior to analysis, both the spectrometer and the ATR accessory were flushed with dry nitrogen, and all samples were placed in a desiccator with P_2O_5 for a week. Three measurements were taken for each sample.

2.2.4. X-ray diffraction (XRD) analysis

An X'Pert Pro diffractometer, manufactured by Philips in Eindhoven, the Netherlands, was utilized for XRD (X-ray diffraction) studies. The operating parameters of the diffractometer were set as follows: voltage at 40 kV, current at 30 mA, and scanning speed at 0.02°/s. CuKα radiation with a wavelength of 0.15405 nm was used for the diffraction experiments. The range of the diffraction spectrum obtained was from 10° to 40°. Before testing, the cellulose samples were dried using compressed air. The obtained diffractograms were analyzed to determine the degree of cellulose crystallinity (crystallinity index, Cr.I.), as well as the size of the crystallites and the residual stresses present in the crystallites. To calculate the degree of cellulose crystallinity, the following formula [30] was used:

$$Cr.I. = [(I_{200} - I_{am})/I_{200}] \times 100 \quad (1)$$

In the formula, I_{200} represents the intensity of the peak in the diffractogram at an angle 2θ approximately 23°, and I_{am} denotes the intensity for amorphous cellulose at an angle between 2θ of 18° to 19° (considered as the baseline). For this study, the intensity of I_{am} was assumed to be equal to the background intensity at an angle 2θ = 18.5°.

To determine $I\alpha/I\beta$ ratio, the surface area under the peak corresponding to the crystallographic plane (100) was divided by the surface area under the peak corresponding to the (200) plane. These results compare to $I\alpha/I\beta$ ratio that were determined by M. Wada et.al [31] which is shown below. To determine the $I\alpha/I\beta$ ratio the following formulas were used:

$$d_1 = 0,613*0,1x + 0,602*0,1y \quad (2)$$

$$d_2 = 0,535*0,1y + 0,529*0,1x \quad (3)$$

where: d_1, d_2 – d-spacing from two phases. The above formula is true when Iα/Iβ ratio is x/y and $x + y = 10$.

To determine the dominant allomorph the following formula was used:

$$Z = 1693*d_1 - 902*d_2 - 549 \quad (4)$$

If Z > 0 means that BNC is Iα-rich.

To determine the residual stresses in the crystallites and the size of the crystallites, Williamson-Hall analysis was performed. The widths of each of the three peaks at half peak height were determined. The peaks were approximated using the Lorentz function in the Origin program, employing the nonlinear least squares method. The total half-width of the peaks (B), expressed in radians, is considered as the result of the deformation of the crystal lattice (ε) caused by the residual stress (σ_R) and the size of the crystallites (L), as well as the instrumental broadening of the test device. This relationship can be written as follows [32]:

$$B\sin\theta = (a_s \cdot \lambda)/L + 4\varepsilon \cdot \sin\theta + B_I \cdot \sin\theta \quad (5)$$

In the equation, a_s represents Sherrer's constant, which depends on the shape and distribution of the crystallites. For an ideal set of 1D linear crystals, Scherrer's constant is typically assumed to be $a_s = 0.88$ [33]. B_I represents the instrumental broadening, which was evaluated using a silicon standard. For this analysis, the instrumental broadening was assumed to be 10 % of the total peak broadening.

2.2.5. Nanoindentation test

The Nano Test Vantage nanoindenter, manufactured by Micro Materials in the UK, was utilized for nanohardness testing. The testing

Table 2
Results of ANOVA statistical analysis.

		Sum of squares SS			df	Average square			F			Significance level
		H	E	ε		H	E	ε	H	E	ε	
BNC	Among groups	0.118	34.56	4E−05	3	0.039	11.52	1.30E−05	8.56	20.54	13.96	0.01
	Within groups	0.17	20.75	3E−05	37	0.005	0.56	9.34E−07				
	Total	0.288	55.31	7E−05	40							
BNC/HA	Among groups	0.363	52.63	0.033	3	0.121	17.54	0.011	11.1	15.49	154.1	0.01
	Within groups	0.405	41.91	0.003	37	0.011	1.133	7.0E−05				
	Total	0.768	94.54	0.036	40							

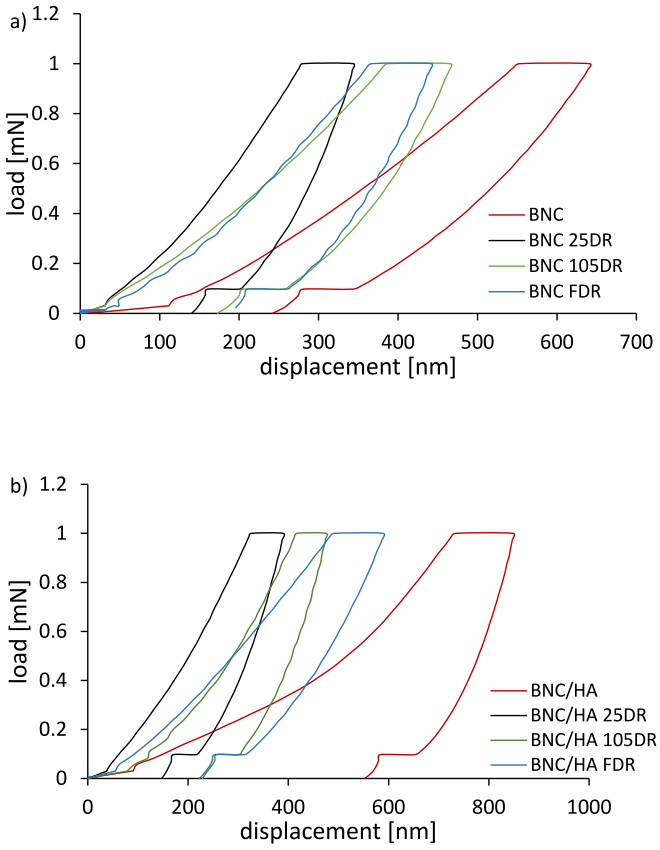

Fig. 8. Load - displacement curves determined for physically modified BNC - 9a) and BNC HA - 9b). The curves shown are the median of 10 measurements.

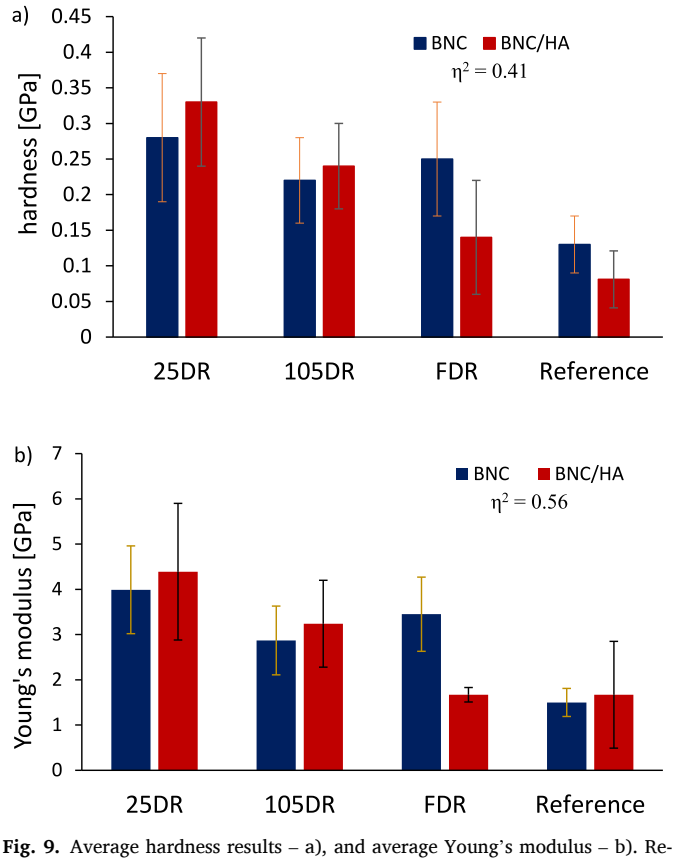

Fig. 9. Average hardness results – a), and average Young's modulus – b). Results obtained in ten measurements in the nanoindentation test. Error bars indicate ± average standard deviation. η^2 - power factor of significance of differences.

involved the use of a diamond indenter in the shape of a three-sided Berkovich pyramid. The maximum load applied during the test was 1 mN, and both the loading and unloading rates were set at 0.02 μN/s. To determine the strain rate (cellulose creep), the maximum load was maintained for a dwell time of 10 s. The creep rate ($\dot{\varepsilon} = d\varepsilon/dt$) was calculated as the slope of the straight line representing the relative indenter displacement ε plotted against time t, during the period of stabilized creep (constant creep rate). The hardness and stiffness of cellulose (reduced Young's modulus) were determined using the nanoindentation test, employing the Oliver-Pharr method. According to this method, the hardness (H) is calculated as the ratio of the maximum load (P_{max}), applied during the nanoindentation test to the area of the imprint (A_c), formed in the material in contact with the indenter ($H = P_{max}/A_c$). The stiffness (E) is proportional to the slope of the tangent to the stress relief curve at the point of maximum load (dP/dh), and can be expressed as $E = 0.5(dP/dh)(\pi/A_c)^{0.5}$. Each measurement was repeated 10 times, and the mean values and standard deviations were calculated.

2.2.6. Tensile strength test

The tensile tests were conducted using an Instron C universal tensile machine (Canton, MA, USA). The ASTM modified method D882-00 (ASTM, 2001) was followed to determine the tensile strength (TS) and elongation at break (A) of the specimens. During the tensile tests, the cross-head speed was set to 10 mm/min, and the initial grip separation was maintained at 50 ± 5 mm. The elongation at break (A) was calculated as the ratio of the elongation at the point of sample rupture to the initial length of the sample. The tensile strength (TS) was calculated by dividing the maximum load obtained during the test by the initial cross-sectional area of the sample. The samples used in the tests were strips with dimensions of 15 × 100 mm. For each modified BNC, five tensile tests were performed, and the mean values of TS and A, as well as the standard deviation, were calculated.

2.2.7. Statistical analysis

The average results of mechanical tests were calculated based on at least 5 replications. The obtained data underwent statistical analysis using one-way analysis of variance (ANOVA) to determine significant differences among BNC samples. Significance was accepted at $p < 0.01$.

3. Results and discussion

3.1. BNC characterization by SEM analysis

Surface observations, without the use of a microscope, indicate that both native BNC and freeze-dried BNC have the same thickness and width. These samples exhibit a typical gel and cryo-gel structure. However, SEM observations revealed that during the freezing process preceding freeze-drying, ice crystals formed inside the material, which then expanded and influenced the structure of the resulting cryo-gel. As a result, both BNC and BNC/HA had a higher percentage of pores in their structures after freeze-drying compared to native cellulose. These pores were also larger in size compared to those formed during convection drying. In the study, no additives were used during freezing, resulting in the formation of an open aerogel structure. This structure is likely to possess good water retention properties and exhibits significant swelling capabilities [34] [35]. Convection drying at 25 °C led to a decrease in the width of the samples due to an increase in material thickness. Application of heat at this temperature resulted in the reduction of the outer surface area, pore closure, shrinkage, and the formation of internal hydrogen bonds [11]. Consequently, the dimensions of the pores decreased, as did the area occupied by the pores (Figs. 1–3). Increasing the convection drying temperature to 105 °C further reduced the percentage of pores and their dimensions in the case of BNC. However, in the case of BNC/HA, raising the convection drying temperature to

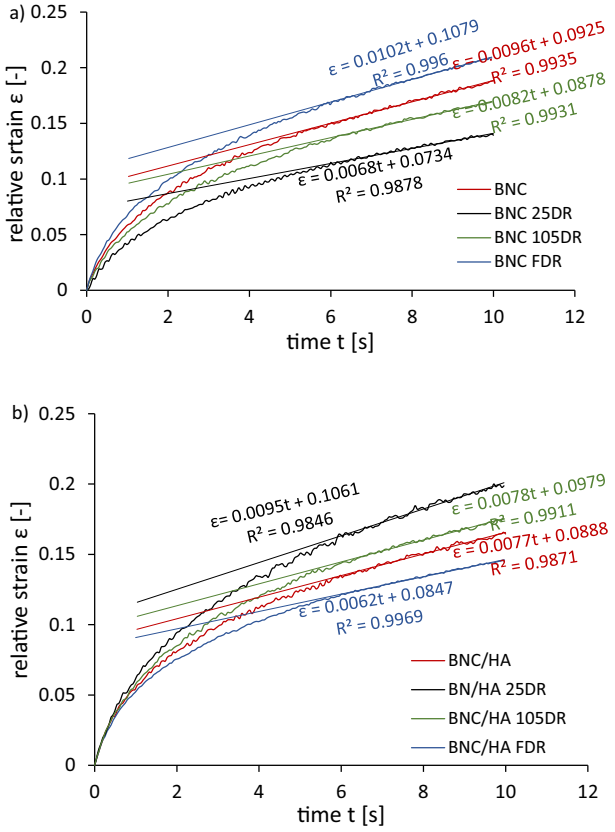

Fig. 10. Examples of creep curves (the median of 10 measurements) determined by the nanoindentation test for BNC - a) and for BNC/HA - b).

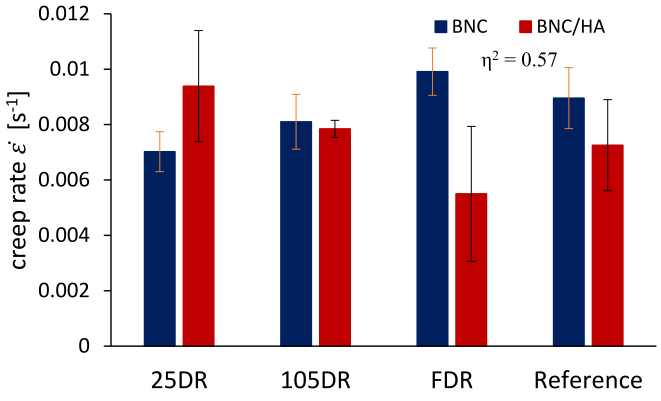

Fig. 11. Average creep rate for BNC and BNC/HA determined from ten tests. Error bars indicate ± standard deviation. η^2 - power factor of significance of differences.

105 °C resulted in an increased pore content, albeit with smaller sizes (Fig. 3b). The analysis of XRD images conducted in Section 3.3 reveals a correlation between the porosity of bacterial cellulose and the magnitude of residual stresses. In the case of the BNC/HA composite, there is a clear relationship between the percentage of pores in the structure and the magnitude of residual stresses. High tensile stresses tend to close the pores, resulting in a reduction in cellulose volume. Conversely, decreasing tensile stresses lead to an increase in porosity within the structure. When compressive stresses are present, such as in the case of BNC 105DR cellulose, pore closure is even more effective than under high tensile stress conditions.

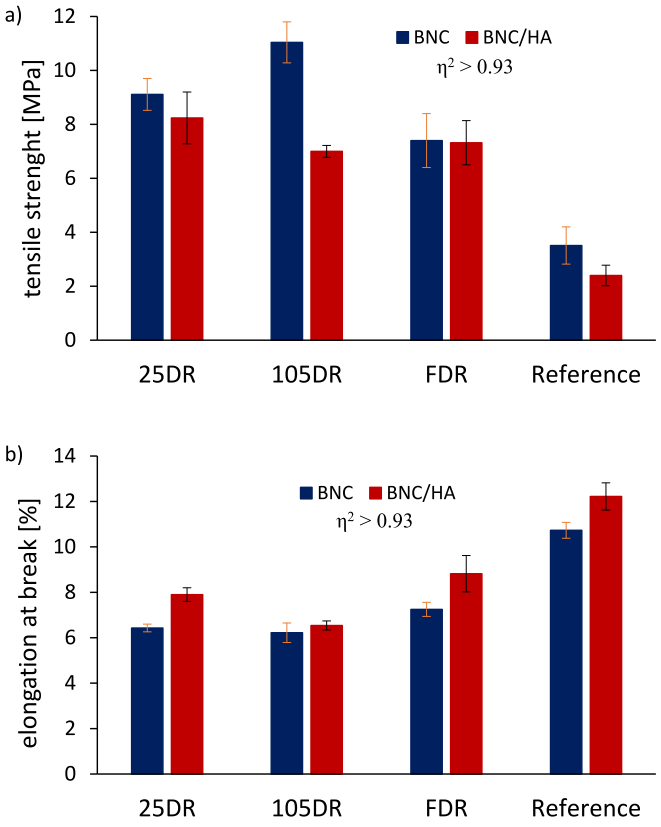

Fig. 12. Tensile strength of BNC and BNC HA – a) and elongation at break of BNC and BNC/HA – b). Error bars indicate ± standard deviation. η^2 - power factor of significance of differences.

3.2. Characteristics of BNC and BNC/HA by Raman spectroscopy

Fig. 4 illustrates the Raman spectra obtained for native BNC and BNC/HA. The Raman spectrum of BNC showed no significant differences due to *in situ* modification with HA. However, a band observed at 3580 cm^{-1} in the BNC spectrum exhibited a shift towards lower wave numbers in the spectrum of BNC/HA. This shift could be interpreted as the formation of new hydrogen bonds between functional groups of BNC and HA. Additionally, a band at 955 cm^{-1} in the BNC spectrum exhibited decreased intensity and broadening in the BNC/HA spectrum, indicating a change in the degree of crystallinity and the size of crystallites [36].

3.3. Characteristic of BNC and BNC/HA by Fourier Transform Infrared Spectroscopy

Differences in the FTIR spectrum between BNC and BNC/HA indicate a higher number of hydrogen bonds in BNC/HA. These differences are observed as increased intensity of the absorption band of the hydroxyl (OH) group in BNC/HA, compared to BNC in the region from 3600 to 3000 cm^{-1}. Addition of hyaluronan also affects the absorption band of the carbonyl (C=O) group at 1645 cm^{-1} in cellulose. Increased intensity of the band and its shift towards lower wavenumbers may suggest the formation of additional hydrogen bonds between the carbonyl groups of hyaluronan and the hydroxyl groups of cellulose. In the case of BNC/HA, changes in absorption bands associated with C-O-C bonds at 1162 cm^{-1}, which are characteristic of cellulose, are also observed. These bands undergo shifts and changes in intensity in the presence of hyaluronan, which may be related to additional hydrogen bonding interactions. Additionally, the appearance of an absorption band associated with amino groups of hyaluronan (NH) at 1544 cm^{-1} suggests the presence of new hydrogen bonds or other interactions between hyaluronan and cellulose (Fig. 5).

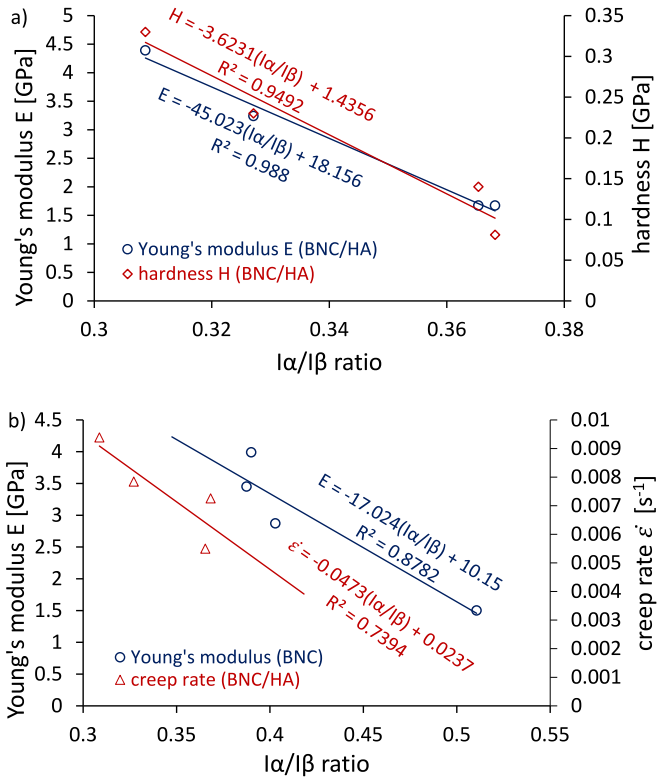

Fig. 13. Effect of the crystalline structure of BNC on its mechanical properties. Correlation between hardness and Young's modulus and *Iα/Iβ* index for BNC/HA - a), and creep rate of BNC/HA, and Young's modulus for BNC *vs Iα/Iβ* index - b).

3.4. Characteristics of BNC and BNC/HA by XRD

Fig. 6 presents the XRD diffraction patterns for BNC (Fig. 6a) and BNC/HA (Fig. 6b). Both patterns exhibit two distinct peaks at approximately 2θ angles of 14.7° and 22.7°, as well as a faint peak at a 2θ angle of around 16.8°. The presence of these distinct peaks indicates the crystalline structure of cellulose. According to [37] BNC produced by the *Komagataeibacter xylinus* strain possesses a crystalline structure corresponding to the *Iα* and *Iβ* phases. The peak at a 2θ angle of 14.7° corresponds to the *Iα* phase with a crystallographic direction of (100), while the peak at a 2θ angle of 22.7° corresponds to the *Iβ* phase with a crystallographic direction of (200) or if the cellulose is *Iα* phase rich 22.7° corresponds to (110). Using formula (4), the value of Z was calculated, and it was found that the following modifications are rich in the *Iα* phase: BNC 25DR, BNC/HA native, BNC/HA 25DR, BNC/HA 105DR and BNC/HA FDR. Crystallographic planes for Iα rich cellulose are marked in the Fig. 6 and the results of the Z values are presented in Table 1.

Table 1 contains the results of the XRD analysis, specifically the calculated *Iα/Iβ* ratios for both BNC and BNC/HA samples. The *Iα/Iβ* ratio represents the relative abundance of the Iα and Iβ phases in the cellulose structure. It can provide insights into the degree of crystallinity and the polymorphic composition of the cellulose material. The information provided suggests that the drying temperature has an impact on the crystalline structure of bacterial cellulose, and the presence of HA molecules further influences this behavior. At low drying temperatures (25DR), the degree of cellulose crystallinity remains constant, suggesting no significant changes in the number of hydrogen bonds between cellulose chains and water molecules. Increasing the drying temperature to 105 °C leads to the breaking of bonds between cellulose chains and water molecules, resulting in a decrease in the spatial ordering of cellulose chains. In the case of the BNC/HA composite, the presence of HA molecules embedded in the cellulose chains allows for the breaking of hydrogen bonds between water molecules and cellulose chains even at a temperature of 25 °C. Consequently, this leads to a reduction in the degree of cellulose crystallinity. However, increasing the drying temperature to 105 °C leads to the breaking of hydrogen bonds between cellulose chains at the sites of embedded hyaluronic acid, allowing for spatial ordering of the chains, and thus increasing the degree of cellulose crystallinity. It is worth noting that in the absence of HA molecules embedded in the cellulose chains, the temperature at which hydrogen bonds between cellulose chains are broken may be higher than 105 °C, making it impossible to increase the degree of crystallinity. As a result, no significant increase in the degree of crystallinity is observed in this case. These observations highlight the influence of drying temperature and the presence of HA molecules on the degree of crystallinity in bacterial cellulose.

The data in Table 1 was used to perform a Williamson-Hall analysis, and the results are presented in Fig. 7. The analysis allowed for the determination of the size of the crystallites (L) and the lattice strain in the crystals (ε). By examining the straight lines in Fig. 7, it is possible to determine the size of the crystallites and the magnitude of residual stresses. In general, BNC produced with the addition of HA exhibits larger crystallite sizes and lower tensile residual stresses compared to native BNC. However, an exception to this trend is observed in BNC convection dried at 105 °C. Increasing the temperature of convection drying leads to larger crystallite sizes, reduced residual stresses, and a shift from tensile to compressive stresses in the case of BNC/HA. Freeze-drying produces crystallites of intermediate size, larger than those produced by convection drying at 25 °C but smaller than those produced after convection drying at 105 °C. Drying at 25 °C does not significantly change the size of the crystallites compared to native BNC but results in an increase in residual stresses of more than twofold. The calculated crystallite sizes are summarized in Table 2. Fig. 7 shows that the relationships $B\sin\theta = (a s\cdot\lambda)/L + 4\varepsilon\cdot\sin\theta$ are linear decreasing functions, indicating the presence of tensile residual stresses in the micro-areas of the crystals. The only exception is the BNC 105DR sample, where compressive residual stresses are observed in the crystals. To accurately determine the value of residual stresses, the knowledge of the longitudinal modulus of elasticity of the crystals is necessary. This information, along with other mechanical properties of BNC and its various modifications, was determined through a nanoindentation test.

Table 3
Effect of *ex situ* and *in situ* modification of BNC and BNC/HA on the mechanical properties.

Modification	L [nm]	σ_R [MPa]	$\dot{\varepsilon} \times 10^{-4}$ [s^{-1}]	E* [GPa]	H [MPa]	TS [MPa]	A [%]
BNC 25DR	3.08	−76.8	70 ± 7	3.99 ± 0.97	0.7 ± 0.08	9.11 ± 0.56	6.43 ± 0.15
BNC 105DR	9.41	10.0	81 ± 10	2.87 ± 0.76	0.22 ± 0.06	11.04 ± 0.98	6.22 ± 0.42
BNC FDR	4.88	−44.9	99 ± 9	3.45 ± 0.82	0.25 ± 0.07	7.40 ± 0.68	7.25 ± 0.32
BNC	2.99	−30.5	90 ± 11	1.5 ± 0.31	0.13 ± 0.04	3.51 ± 0.69	10.73 ± 0.35
BNC/HA 25DR	4.33	−63.9	94 ± 20	4.39 ± 1.51	0.33 ± 0.16	8.24 ± 1.1	7.9 ± 0.34
BNC/HA 105DR	6.99	−7.8	78 ± 3	3.24 ± 0.96	0.23 ± 0.09	7.00 ± 0.25	6.54 ± 0.83
BNC/HA FDR	5.23	−17.5	55 ± 24	1.67 ± 0.16	0.14 ± 0.01	7.32 ± 0.78	8.82 ± 0.21
BNC/HA	4.39	−26.1	73 ± 16	1.67 ± 1.18	0.081 ± 0.09	2.4 ± 0.45	12.22 ± 0.11

3.5. Characteristics of BNC and BNC/HA by nanoindentation test

Fig. 8 displays the load-unload curves obtained for physically modified BNC (Fig. 8a) and BNC/HA (Fig. 8b). The graphs represent the median of 10 measurements. The curves shown in Fig. 8 exhibit typical behavior for elastically plastic materials. In the unloading curves, drift corrections can be observed at 10 % of force. From these curves, Young's modulus, hardness, and creep rate were calculated. Fig. 9 illustrates the results of the calculations. It can be observed that *ex situ* modification of BNC leads to an increase in hardness ranging from 69 % to 115 %, depending on the modification method used. Conversely, double modification of BNC, first *in situ* by adding HA to the medium, and then *ex situ* through soaking in water and convection or freezing drying, allows for a hardness increase ranging from 73 % (in the case of freezing drying) to 407 % (in the case of convection drying at 25 °C). The same trend is observed for the rigidity of BNC (Fig. 9b). *Ex situ* modification increases its stiffness. However, unlike hardness, the addition of HA to the medium enhances the stiffness of BNC. The presence of a significant amount of water in native BNC and BNC/HA likely contributes to a reduction in the modulus of longitudinal elasticity, as observed in the nanoindentation test for physically modified BNC. Only BNC/HA subjected to freeze-drying (FDR BNC/HA) exhibits similar values of Young's modulus (E) and hardness (H) to native BNC and BNC/HA. This outcome is attributed to the size and distribution of pores in the structure of BNC/HA and BNC after freeze-drying, as shown in Fig. 3. Freeze-drying results in the highest percentage of pores and larger pore sizes, compared to other drying methods. It should be noted that due to the application of small forces (1 mN), the obtained results exhibit a large dispersion. The indenter may come into contact with individual filaments, fiber agglomerates, or hit a pore, resulting in calculated hardness values that can be very low or close to zero. However, the results indicate a general trend of increased strength, hardness, and Young's modulus of BNC and BNC/HA after physical modification, compared to the native material. In the case of convection drying of BNC at 25 °C and BNC freeze-drying, a close relationship is observed between the magnitude of residual stresses and high hardness and stiffness, despite the fact that the stresses are tensile in nature. The same correlation is observed for BNC/HA dried at 25 °C. This phenomenon may be attributed to the formation of additional hydrogen bonds, which generate residual tensile stresses. However, no correlation is observed between the degree of crystallinity, size of crystallites, and the hardness and stiffness of BNC.

An important property of BNC, particularly for its use in cardiovascular implants, is its creep resistance. Due to the high stability of cellulose under dynamic loading conditions [38], it was decided to conduct creep tests on BNC only under static loading conditions with a value of 1 mN. Creep resistance is inversely related to the creep rate $\dot{\varepsilon}$ during the steady-state period of dwell time. Fig. 10 illustrates the change in strain ε for modified BNC (Fig. 10a) and BNC/HA (Fig. 10b) during maximum indenter loading. It can be observed that the creep rate decreases for the first 6 s and then stabilizes at a constant level.

Fig. 11 presents the arithmetic mean value of the creep rate calculated from 10 trials. As depicted in Fig. 11, the lowest creep rate is observed for BNC/HA and freeze-dried BNC/HA, while the highest creep rate is recorded for BNC after freeze-drying. These results indicate a relationship between creep resistance and the porosity of BNC. The low number of pores in the structure of BNC/HA and BNC/HA FDR contributes to their favorable creep resistance. Conversely, the high number of pores in BNC FDR cellulose results in low creep resistance. The statistical analysis using one-way analysis of variance (ANOVA) indicates that the obtained results of hardness (H), Young's modulus (E), and creep rate ($\dot{\varepsilon}$) are statistically significant. For all analyzed cases of BNC modification, significant differences were observed between groups with a *p*-value of <0.01. The strength of these effects was further evaluated using the η^2 coefficient, which is calculated as the ratio of the sum of squares (SS) among groups to the total SS. The η^2 coefficient values for both groups of BNC and BNC/HA cellulose were not <0.41, 0.56, and 0.57 for hardness, Young's modulus, and creep rate, respectively. As the η^2 values exceeded 0.14, it can be concluded that there is a strong differentiation effect between the BNC groups.

3.6. BNC characterization by tensile strength test

Fig. 12 presents the results of the effect of *in situ* chemical and *ex-situ* physical modification (dehydration/rehydration) on the tensile strength (TS) and elongation (A) of BNC and BNC/HA. Comparing BNC and BNC/HA, it can be observed that the tensile strength is higher for BNC, both in its native form and after *ex situ* modification. Several explanations can be considered for this phenomenon:

1. After the addition of HA to the culture medium, the fibrils may adhere to each other, possibly through the incorporation of HA between them.
2. HA penetration inside the cellulose network may fill the space and maintain close interaction between the nanofibrils [39].
3. HA, being a natural substance, may not possess adequate mechanical properties, and its addition to the nutrient medium could weaken the resulting structure.

In addition to the above factors, TS is influenced by residual stresses and the size, number, and dimensions of pores in the cellulose microstructure. The highest TS was demonstrated by BNC without HA after convection drying at 105 °C, where the residual stresses were compressive. BNC 25DR also exhibited high TS, which can be attributed to the low porosity of the structure and small pore dimensions. In the case of *in situ* HA-modified BNC, convection-dried BNC at 25 °C showed the highest TS, despite the presence of the highest residual tensile stresses. In this case, the low porosity and absence of larger-sized pores played a significant role. The decrease in drying temperature also contributed to the increase in TS of BNC and BNC/HA, possibly due to the formation of more hydrogen bonds within the BNC fibers and changes in the spatial structure of the BNC polysaccharide chains [40]. The strong packing of fibers reinforced with hydrogen bonds limits the mobility of the polymer chains and consequently increases the strength of BNC [41]. Fig. 11 demonstrates that BNC without added HA, conventionally dried at 25 °C and 105 °C, exhibited the lowest creep rate, indicating lower mobility of polysaccharide chains and higher strength. Slightly lower TS values were observed for FDR BNC and FDR BNC/HA, which may be associated with larger pore sizes (Fig. 3). However, the elongation (A) was slightly higher for these modifications, suggesting better water absorption and swelling properties of FDR BNC/HA [35]. The obtained tensile strength (TS) values for both *ex situ* modified BNC and BNC/HA are generally above 7 MPa, which is considered a sufficient value for the potential use of BNC or BNC/HA as a biomaterial for the aortic valve. This is noteworthy since the TS of aortic petals and the aorta itself does not exceed 5 MPa [42].

The statistical analysis using one-way analysis of variance (ANOVA) indicates that the significance level of the results for each BNC group is higher than 0.01, suggesting that the observed differences in TS and elongation (A) values between the groups are statistically significant. Moreover, the η^2 coefficient values, which represent the effect size, are >0.93, indicating a strong differentiation effect between the BNC groups. This reinforces the conclusion that the modifications applied to BNC have a significant impact on its mechanical properties, particularly in terms of TS and A. Table 2 below presents the details of the statistical analysis.

3.7. Relationship between the mechanical properties of BNC and its crystal structure

The analysis reveals that in some cases of *ex situ* modification of BNC, there is a linear correlation between mechanical properties (hardness, stiffness) and the crystal structure represented by the Iα/Iβ index.

Fig. 13a demonstrates that the hardness and stiffness of *ex situ*-modified BNC/HA show linear relationships with the $I\alpha/I\beta$ index. A higher number of type $I\beta$ crystals in the BNC structure corresponds to increased strength properties. Similarly, Fig. 13b shows a correlation between the creep rate and crystal structure, indicating that an increased number of $I\beta$ crystals leads to a lower creep rate in BNC/HA cellulose. This can be attributed to the denser packing of $I\beta$ crystals, which reduces chains mobility and enhances resistance to creep. It is observed that *ex situ* modified BNC/HA generally has fewer $I\beta$ crystals compared to BNC, resulting in lower strength properties. However, it is important to note that the mechanical properties are influenced by various factors, including crystal structure, pore size and distribution, and residual stress. The influence of crystallite size on the mechanical properties of BNC was not observed. Table 3 summarizes all the properties of *in situ* and *ex situ* modified BNC, including crystallite size and residual stresses. The lack of a simple relationship between crystallite size and residual stresses suggests that crystallite type, pore distribution and size, and other factors play a more significant role in determining the mechanical properties of BNC.

Based on the obtained results, one particular modification approach (BNC dried at 25 °C and rehydration) was selected for further bioassays. These subsequent tests assessed the biodegradability of the modified bacterial cellulose in the presence of *S. aureus*, *C. albicans*, and *A. fumigatus* [43]. The six-month tests demonstrated the favorable resistance of bacterial biocellulose, and additional evaluations such as Shima's test indicated its low hemolysis index and low thrombogenicity [14].

4. Limitations and future perspectives

The presented research results should be subjected to critical evaluation. The analysis of porosity was determined using the principles of quantitative metallography, which state that the volumetric, surface, linear, and point fractions are equal. Consequently, the SEM image was represented as a binary image of pores. To obtain the actual pore distribution throughout the sample, it would be necessary to conduct examinations using techniques such as computer tomography or the Brunauer-Emmett-Teller (BET) method. The Williamson-Hall analysis, presented to obtain second-order stress quantities and crystallite sizes, relies on the full width at half maximum (FWHM), which, depending on the chosen peak distribution function (Gaussian, Lorentzian, pseudo-Voigt, or Voigt), may take different values. Also, the shapes of the crystallites are not fully known; not all necessarily assume the same form. Depending on their shapes, the Sherrer constant is selected for calculations.

The obtained modifications of BNC and BNC/HA meet the requirements of mechanical properties obtained in the tensile test. The next step is to design the heart valve, sew it, and perform *in vitro* testing on a measuring station where it will be possible to determine the effective opening area of the valve and to conduct fatigue tests. And the final step will involve conducting *in vivo* studies on animals.

5. Conclusion

The obtained results indicate that the addition of hyaluronic acid decreases the degree of crystallinity and increases crystal size in BNC. Moreover, HA promotes the formation of hydrogen bonds between cellulose and hyaluronic acid chains, resulting in increased hardness, stiffness, and resistance to creep of the modified bacterial cellulose.

Chemical modification also leads to a reduction in residual stresses within the crystal lattice of the modified BNC. On the other hand, *ex situ* modification of both BNC and BNC/HA increases hardness, stiffness, and tensile strength while reducing elongation at break in tensile tests. The obtained modifications of BNC meet the requirements of mechanical properties obtained in the tensile test.

The authors declare no competing financial interests. The project is carried out in collaboration of scientific and research institutions including the Medical University of Gdańsk, Faculty of Medicine, Bowil Biotech *Sp.* z o.o. Gdańsk University of Technology, Faculty of Chemistry, Faculty of Mechanical Engineering, Ship Technology of the Gdańsk University of Technology, Maritime Advanced Research Centre S.A. The Foundation for Cardiac Surgery of Prof. Zbigniew Religa, University of Gdańsk, Faculty of Biology. Name and number of the project: KARDIO BNC PBS2/A7/16/2013. Narodowe Centrum Badań i Rozwoju (NCBiR) - Grant PBS2/A7/16/2013 and grant number: 2/1/2022/IDUB/I3b/Ag: "The impact of silver nanoparticles on the mechanical and biological properties of a nanocomposite based on bacterial cellulose: application in cardiothoracic surgery and dermatology." The sponsor had no involvement in the design of the study; in the collection, analysis and interpretation of the data; in the writing of the report; and in the decision to submit the article for publication.

CRediT authorship contribution statement

Alicja Stanisławska: Writing – original draft, Visualization, Investigation, Data curation. **Marek Szkodo:** Writing – review & editing, Writing – original draft, Visualization, Methodology, Data curation, Conceptualization. **Hanna Staroszczyk:** Writing – review & editing, Conceptualization. **Kinga Dawidowska:** Visualization, Investigation. **Magdalena Kołaczkowska:** Project administration. **Piotr Siondalski:** Validation, Supervision, Funding acquisition.

Declaration of competing interest

The authors declare the following financial interests/personal relationships which may be considered as potential competing interests: Alicja Stanislawska reports financial support was provided by Gdansk University of Technology Faculty of Ocean Engineering and Ship Technology. Piotr Siondalski reports financial support was provided by Medical University of Gdansk. Alicja Stanislawska, Marek Szkodo, Hanna Staroszczyk, Kinga Dawidowska, Magdalena Kolaczkowska, Piotr Siondalski has patent #PL 242163 B1 issued to Not applicable. Alicja Stanislawska, Marek Szkodo, Hanna Staroszczyk, Kinga Dawidowska, Magdalena Kolaczkowska, Piotr Siondalski has patent #EP3876869A1 pending to Not applicable. Alicja Stanislawska, Marek Szkodo, Hanna Staroszczyk, Kinga Dawidowska, Magdalena Kolaczkowska, Piotr Siondalski has patent #US20220001078 pending to Not applicable. Alicja Stanislawska, Marek Szkodo, Hanna Staroszczyk, Kinga Dawidowska, Magdalena Kolaczkowska, Piotr Siondalski has patent #WO/2020/096469 pending to Not applicable. If there are other authors, they declare that they have no known competing financial interests or personal relationships that could have appeared to influence the work reported in this paper.

References

[1] D. Klemm, F. Kramer, S. Moritz, T. Lindström, M. Ankerfors, D. Gray, A. Dorris, Nanocelluloses: a new family of nature-based materials, Angew. Chem. Int. Ed. 50 (24) (2011) 5438–5466, https://doi.org/10.1002/anie.201001273.
[2] G. Patterson, Cellulose before CELL: historical themes, Carbohydr. Polym. 252 (2021) 117182-89, https://doi.org/10.1016/j.carbpol.2020.117182.
[3] S.M. Choi, K.M. Rao, S.M. Zo, E.J. Shin, S.S. Han, Bacterial cellulose and its applications, Polymers 14 (6) (2022) 1080–1124, https://doi.org/10.3390/polym14061080.
[4] S. Gorgieva, J. Trček, Bacterial cellulose: production, modification and perspectives in biomedical applications, Nanomaterials 9 (10) (2019) 1352–1372, https://doi.org/10.3390/nano9101352.
[5] M. Pang, Y. Huang, F. Meng, Y. Zhuang, H. Liu, M. Du, Q. Ma, Q. Wang, Z. Chen, L. Chen, T. Cai, Y. Cai, Application of bacterial cellulose in skin and bone tissue engineering, Eur. Polym. J. 122 (2020) 109365-96, https://doi.org/10.1016/j.eurpolymj.2019.109365.
[6] T. Su, N. Liu, D. Lei, L. Wang, Z. Ren, Q. Zhang, J. Su, Z. Zhang, Y. Gao, Flexible MXene/bacterial cellulose film sound detector based on piezoresistive sensing mechanism, ACS Nano 16 (5) (2022) 8461–8471, https://doi.org/10.1021/acsnano.2c03155.
[7] H. Suryanto, M. Muhajir, T. Sutrisno, N. Mudjiono, U. Yanuhar Zakia, The mechanical strength and morphology of bacterial cellulose films: the effect of

NaOH concentration, in: IOP Conference Series: Materials Science and Engineering, IOP Publishing, 2019, https://doi.org/10.1088/1757-899X/515/1/012053 (pp. 012053-61).
[8] P. Cazón, G. Velázquez, M. Vázquez, Bacterial cellulose films: evaluation of the water interaction, food Packag. Shelf, Life 25 (2020) 100526-36, https://doi.org/10.1016/j.fpsl.2020.100526.
[9] F.G. Blanco Parte, S.P. Santoso, C.-C. Chou, V. Verma, H.-T. Wang, S. Ismadji, K.-C., Cheng, current progress on the production, modification, and applications of bacterial cellulose, Crit. Rev. Biotechnol. 40 (3) (2020) 397–414, https://doi.org/10.1080/07388551.2020.1713721.
[10] M.P. Illa, C.S. Sharma, M. Khandelwal, Tuning the physiochemical properties of bacterial cellulose: effect of drying conditions, J. Mater. Sci. 54 (18) (2019) 12024–12035, https://doi.org/10.1007/s10853-019-03737-9.
[11] M. Beaumont, J. König, M. Opietnik, A. Potthast, T. Rosenau, Drying of a cellulose II gel: effect of physical modification and redispersibility in water, Cellulose 24 (2017) 1199–1209, https://doi.org/10.1007/s10570-016-1166-9.
[12] A. Stanisławska, H. Staroszczyk, M. Szkodo, The effect of dehydration/rehydration of bacterial nanocellulose on its tensile strength and physicochemical properties, Carbohydr. Polym. 236 (2020) 116023-32, https://doi.org/10.1016/j.carbpol.2020.116023.
[13] J. Singh, T.W. Steele, S. Lim, Bacterial cellulose adhesive patches designed for soft mucosal interfaces, Biomater. Adv. 144 (2023) 213174, https://doi.org/10.1016/j.bioadv.2022.213174.
[14] M. Kołaczkowska, P. Siondalski, M.M. Kowalik, R. Pęksa, A. Długa, W. Zając, P. Dederko, I. Kołodziejska, E. Malinowska-Pańczyk, I. Sinkiewicz, H. Staroszczyk, A. Śliwińska, A. Stanisławska, M. Szkodo, P. Pałczyńska, G. Jabłoński, A. Borman, P. Wilczek, Assessment of the usefulness of bacterial cellulose produced by Gluconacetobacter xylinus E25 as a new biological implant, Mater. Sci. Eng. C 97 (2019) 302–312, https://doi.org/10.1016/j.msec.2018.12.016.
[15] H. Zhao, L. Zhang, S. Zheng, S. Chai, J. Wei, L. Zhong, Y. He, J. Xue, Bacteriostatic activity and cytotoxicity of bacterial cellulose-chitosan film loaded with in-situ synthesized silver nanoparticles, Carbohydr. Polym. 281 (2022) 119017, https://doi.org/10.1016/j.carbpol.2021.119017.
[16] L. Ji, F. Zhang, L. Zhu, J. Jiang, An in-situ fabrication of bamboo bacterial cellulose/sodium alginate nanocomposite hydrogels as carrier materials for controlled protein drug delivery, Int. J. Biol. Macromol. 170 (2021) 459–468, https://doi.org/10.1016/j.ijbiomac.2020.12.139.
[17] L. Liu, X. Ji, L. Mao, L. Wang, K. Chen, Z. Shi, A.A.Q. Ahmed, S. Thomas, R. V. Vasilievich, L. Xiao, Hierarchical-structured bacterial cellulose/potato starch tubes as potential small-diameter vascular grafts, Carbohydr. Polym. 281 (2022) 119034-47, https://doi.org/10.1016/j.carbpol.2021.119034.
[18] A. Sommer, P. Dederko-Kantowicz, H. Staroszczyk, S. Sommer, M. Michalec, Enzymatic and chemical cross-linking of bacterial cellulose/fish collagen composites—a comparative study, Int. J. Mol. Sci. 22 (7) (2021) 3346–3366, https://doi.org/10.3390/ijms22073346.
[19] F. Torres, J. Arroyo, O. Troncoso, Bacterial cellulose nanocomposites: an all-nano type of material, Mater. Sci. Eng. C 98 (2019) 1277–1293, https://doi.org/10.1016/j.msec.2019.01.064.
[20] F. Wahid, L.-H. Huang, X.-Q. Zhao, W.-C. Li, Y.-Y. Wang, S.-R. Jia, C. Zhong, Bacterial cellulose and its potential for biomedical applications, Biotechnol. Adv. 53 (2021) 107856-87, https://doi.org/10.1016/j.biotechadv.2021.107856.
[21] M. Ul-Islam, F. Ahmad, A. Fatima, N. Shah, S. Yasir, M.W. Ahmad, S. Manan, M. W. Ullah, Ex situ synthesis and characterization of high strength multipurpose bacterial cellulose-aloe vera hydrogels, Front. Bioeng. Biotechnol. 9 (2021) 601988-99, https://doi.org/10.3389/fbioe.2021.601988.
[22] X. Wang, J. Tang, J. Huang, M. Hui, Production and characterization of bacterial cellulose membranes with hyaluronic acid and silk sericin, Colloids Surf. B Biointerfaces 195 (2020) 111273-80, https://doi.org/10.1016/j.colsurfb.2020.111273.
[23] Y. Luo, G. Li, L. Chen, F.F. Hong, Preparation and evaluation of bacterial Nanocellulose/hyaluronic acid composite artificial cornea for application of corneal transplantation, Biomacromolecules 24 (1) (2023) 201–212, https://doi.org/10.1021/acs.biomac.2c01052.
[24] S. Tang, K. Chi, H. Xu, Q. Yong, J. Yang, J.M. Catchmark, A covalently cross-linked hyaluronic acid/bacterial cellulose composite hydrogel for potential biological applications, Carbohydr. Polym. 252 (2021) 117123-33, https://doi.org/10.1016/j.carbpol.2020.117123.
[25] T.D. Lopes, I.C. Riegel-Vidotti, A. Grein, C.A. Tischer, P.C.d.S. Faria-Tischer, Bacterial cellulose and hyaluronic acid hybrid membranes: production and characterization, Int. J. Biol. Macromol. 67 (2014) 401–408, https://doi.org/10.1016/j.ijbiomac.2014.03.047.
[26] M.A. Hassan, T.M. Tamer, K. Valachová, A.M. Omer, M. El-Shafeey, M.S. Mohy Eldin, L. Šoltés, Antioxidant and antibacterial polyelectrolyte wound dressing based on chitosan/hyaluronan/phosphatidylcholine dihydroquercetin, Int. J. Biol. Macromol. 166 (2021) 18–31, https://doi.org/10.1016/j.ijbiomac.2020.11.119.
[27] D.J. Kodavaty, A. Deshpande, Mechanical and swelling properties of poly (vinyl alcohol) and hyaluronic acid gels used in biomaterial systems - a comparative study, Def. Sci. J. 64 (2014) 222–229, https://doi.org/10.14429/dsj.64.7320.
[28] S. Fooladi, M.H. Nematollahi, N. Rabiee, S. Iravani, Bacterial cellulose-based materials: a perspective on cardiovascular tissue engineering applications, ACS Biomater Sci. Eng. (2023) 2949–2969, https://doi.org/10.1021/acsbiomaterials.3c00300.
[29] S. Jakmuangpak, T. Prada, W. Mongkolthanaruk, V. Harnchana, S. Pinitsoontorn, Engineering bacterial cellulose films by nanocomposite approach and surface modification for biocompatible triboelectric Nanogenerator, ACS Appl. Electron. Mater. 2 (8) (2020) 2498–2506, https://doi.org/10.1021/acsaelm.0c00421.
[30] L. Segal, J.J. Creely, A.E. Martin, C.M. Conrad, An empirical method for estimating the degree of crystallinity of native cellulose using the X-ray diffractometer, Text. Res. J. 29 (10) (1959) 786–794, https://doi.org/10.1177/004051755902901003.
[31] M. Wada, T. Okano, J. Sugiyama, Allomorphs of native crystalline cellulose I evaluated by two equatoriald-spacings, J. Wood Sci. 47 (2) (2001) 124–128, https://doi.org/10.1007/bf00780560.
[32] G.K. Williamson, W.H. Hall, X-ray line broadening from filed aluminium and wolfram, Acta Metall. 1 (1) (1953) 22–31, https://doi.org/10.1016/0001-6160(53)90006-6.
[33] A.L. Patterson, The Scherrer formula for X-ray particle size determination, Phys. Rev. 56 (10) (1939) 978–982, https://doi.org/10.1103/PhysRev.56.978.
[34] J. Han, C. Zhou, Y. Wu, F. Liu, Q. Wu, Self-assembling behavior of cellulose nanoparticles during freeze-drying: effect of suspension concentration, Particle Size, Crystal Structure, and Surface Charge, Biomacromolecules 14 (5) (2013) 1529–1540, https://doi.org/10.1021/bm4001734.
[35] F. Jiang, D.M. Dinh, Y.-L. Hsieh, Adsorption and desorption of cationic malachite green dye on cellulose nanofibril aerogels, Carbohydr. Polym. 173 (2017) 286–294, https://doi.org/10.1016/j.carbpol.2017.05.097.
[36] J.H. Wiley, R.H. Atalla, Band assignments in the Raman spectra of celluloses, Carbohydr. Res. 160 (1987) 113–129, https://doi.org/10.1016/0008-6215(87)80306-3.
[37] A. Vazquez, M.L. Foresti, P. Cerrutti, M. Galvagno, Bacterial cellulose from simple and low cost production media by Gluconacetobacter xylinus, J. Polym. Environ. 21 (2) (2013) 545–554, https://doi.org/10.1007/s10924-012-0541-3.
[38] J. Poustis, C. Baquey, D. Chauveaux, Mechanical properties of cellulose in orthopaedic devices and related environments, Clin. Mater. 16 (2) (1994) 119–124, https://doi.org/10.1016/0267-6605(94)90106-6.
[39] K.M. Lopez, S. Ravula, R.L. Pérez, C.E. Ayala, J.N. Losso, M.E. Janes, I.M. Warner, Hyaluronic Acid–Cellulose Composites as Patches for Minimizing Bacterial Infections, ACS Omega 5(8) (2020) 4125–4132. doi:https://doi.org/10.1021/acsomega.9b03852.
[40] M. Ul-Islam, T. Khan, J.K. Park, Water holding and release properties of bacterial cellulose obtained by in situ and ex situ modification, Carbohydr. Polym. 88 (2) (2012) 596–603, https://doi.org/10.1016/j.carbpol.2012.01.006.
[41] R. Velmurugan, T.P. Mohan, Epoxy-clay nanocomposites and hybrids: synthesis and characterization, J. Reinf. Plast. Compos. 28 (1) (2008) 17–37, https://doi.org/10.1177/0731684407081439.
[42] K. Dawidowska, A. Stanisławska, Influence of preservative on the tensile strength of the tissue of porcine circulatory system, Adv. Mater. Sci. 15 (2015) 67–75, https://doi.org/10.1515/adms-2015-0017.
[43] P. Dederko, E. Malinowska-Panczyk, H. Staroszczyk, I. Sinkiewicz, P. Szweda, P. Siondalski, In vitro biodegradation of bacterial nanocellulose under conditions simulating human plasma in the presence of selected pathogenic microorganisms, Polimery/Polymers 63 (5) (2018) 372–380, https://doi.org/10.14314/polimery.2018.5.6.